Computations of soot formation in ethylene/air counterflow diffusion flames and its interaction with radiation

I. Hernández [a], G. Lecocq [a] D. Poitou [a] E. Riber [a] B. Cuenot [a]

[a] *CERFACS, 42, Avenue Gaspard Coriolis, 31057 Toulouse, France.*

Received *****; accepted after revision +++++

Presented by I. Hernández

Abstract

A methodology is presented which allows to predict soot levels produced in simple, one-dimensional laminar flames. The method is applied to the calculation of a set of well documented ethylene/air counterflow diffusion flames, using a detailed chemical mechanism [21] and a semi-empirical, two-equation soot model from Leung *et al.* [1]. Modifications of the original soot model are made in order to retrieve the experimental measurements of Hwang & Chung [14]. To account for radiative heat losses, a second series of fully coupled gas/soot/radiation simulations of the counterflow flames is performed. This allows to assess the effect of soot and gas radiation on soot formation and on the flame structure.

Résumé

Calcul de la formation des suies sur des flammes de diffusion à contre-courant de éthylène/air. Une méthodologie est proposée pour le calcul des niveaux de suies produits dans des flammes laminaires mono-dimensionnelles. Cette méthode est appliquée à une série de flammes de diffusion à contre-courant éthylène/air, largement référencées et documentées dans la littérature, et calculées avec un mécanisme chimique détaillé [21] et le modèle semi-empirique à deux équations de Leung *et al.* [1]. Le modèle de suie a été corrigé afin d'obtenir un meilleur accord avec les mesures expérimentales de Hwang & Chung [14]. Afin de prendre en compte les pertes thermiques radiatives, une deuxième série de simulations couplées gaz/suies/rayonnement de ces flammes à contre-courant a été réalisée. Cette démarche permet d'évaluer l'effet du rayonnement des suies et de la phase gazeuse sur la formation des suies et sur la structure de flamme.

Key words: soot ; radiation ; counterflow diffusion flames

Mots-clés : suies ; rayonnement ; flammes de diffusion à contre-courant

Email address: hernand@cerfacs.fr (I. Hernández).

Version française abrégée

Une série des flammes de diffusion à contre-courant d'éthylène/air avec une concentration variable en oxygène au côté oxydant est calculée à l'aide d'un code monodimensionnel et une chimie détaillée. La même tendance est observée que dans la littérature : les valeurs maximales de température et de concentration d'acetylène sont d'autant plus elevées que la concentration en oxygène dans les flammes est grande. Les profils de suies correspondant à ces flammes sont calculés avec un solveur développé a cet effet basé sur le modèle de formation et d'oxydation des suies semi-empirique à deux équations de Leung *et al.* [1]. Les niveaux de suies les plus importants sont prédits dans les flammes où les valeurs de température et concentration d'acetylène sont les plus importantes. Ceci montre un bon accord qualitatif avec les mesures expérimentales, les valeurs maximales de fraction volumique de suies étant sous-estimées. Le modèle de suies est ensuite ajusté pour retrouver un meilleur accord avec les valeurs expérimentales. Finalement, les pertes thermiques par rayonnement sont incluses dans le calcul en utilisant un solveur radiatif basé sur la méthode des ordonnées discrètes avec un modèle spectral détaillé. Des simulations couplées gaz/suies/rayonnement des flammes permettent d'évaluer l'effet du rayonnement sur les structures des flammes. Le rayonnement dû aux suies est identifié comme étant plus important que la contribution associée à la phase gazeuse. Le rayonnement a pour effet de diminuer la température des flammes, comme attendu. Aussi, la quantité de suies produite est plus faible lorsque le rayonnement est pris en compte dû à la diminution du pic de température dans les flammes.

1. Introduction

Prediction of soot emission by flames remains a difficult challenge for combustion simulations and, in most cases, is simply neglected. However, there are numerous reasons to account for soot formation in flames [2,3]. Soot present in the exhaust gases of commercial aircrafts engines may change the physico-chemistry of the atmosphere: they are suspected to trigger the nucleation of cirrus clouds [4], which in turn changes the climate in high air traffic zones as a result of a radiative balance. The exhaust gases released at ground level from vehicles (mainly Diesel engines) contain soot particles, which are hazardous for human health [5]. Soot also plays a major role in industrial furnaces or boilers, where the purpose is to maximize the heat exchange through radiation to a load. In this sense, soot particles are desirable within the furnace, but unwanted at the outlet [6]. This poses technical challenges to designers, which can only be overcome with accurate predictions of soot formation in combustion systems.

Soot production is a very complicated phenomenon involving many chemical reactions and physical mechanisms which are still not fully understood [7,8]. It is widely accepted [9] that acetylene acts as a precursor for soot formation. However, many intermediate steps are also important for soot formation. Polycyclic aromatic hydrocarbons (PAH) are formed from C_2H_2 and a symple cycle C_6H_6. They combine together or with C_2H_2 to form larger PAH and, finally, an incipient soot particle. These particles may grow bigger by the addition of other hydrocarbons or by coalescence to form larger soot particles, they can also be destroyed by oxidation reactions [8]. Furthermore, soot chemistry is highly dependent on temperature. Hence, soot-driven radiative losses must be accounted for if accurate predictions are sought.

There are many soot formation and oxidation models available in the literature and, according to Kennedy [7], they can be classified in order of growing complexity as empirical, semi-empirical and detailed models. Semi-empirical models [10,11,12,13,1] are conceived to predict soot levels for a particular parent fuel and type of flame, according to which their numerical parameters are tuned. Although they

include some physics, their predictive performance is limited to the flame they are adjusted to reproduce. They remain however the best choice when quick estimations of soot levels are sought.

The objective of the present work is to evaluate the behaviour of a soot model on academic configurations and to establish a methodology for a systematic testing of different soot models and chemical mechanisms. A semi-empirical soot model with only two transport equations has been selected in view of its future implementation in a 3D solver for its application in industrial configurations. The configuration studied corresponds to a series of counterflow diffusion flames formed between opposed round jets of ethylene and air experimentally characterized by Hwang & Chung [14].

2. Methodology

2.1. *Governing equations*

The mass, momentum, energy and chemical species conservation equations corresponding to the two-dimensional, axisymmetric problem of two opposed jets are solved. The problem is transformed into a one-dimensional problem by solving the equations along the streamline passing through the stagnation point and the resulting equations are presented in [15].

2.2. *Soot model*

The semi-empirical model proposed by Leung *et al.* [1] has been chosen, as it provides good estimations of the soot levels at a low computational cost [16,17,18], then allowing a further use in complex geometries [19]. This soot model considers two transported variables, the soot mass fraction Y_s and the soot particle number density n, and C_2H_2 is taken as the soot precursor. Their conservation equations are:

$$\frac{\partial \rho Y_s}{\partial t} + \frac{\partial \rho Y_s u_i}{\partial x_i} = -\frac{\partial}{\partial x_i}\left(\rho Y_s V_{t,i}\right) + \dot{\omega}_s'' \tag{1}$$

$$\frac{\partial}{\partial t}\left(\rho \frac{n}{N_A}\right) + \frac{\partial}{\partial x_i}\left(\rho \frac{n}{N_A} u_i\right) = -\frac{\partial}{\partial x_i}\left(\rho \frac{n}{N_A} V_{t,i}\right) + \dot{\omega}_n'' \tag{2}$$

where ρ is the density, u_i is the velocity in the i direction and $N_A = 6.022 \cdot 10^{26}\,[particles/kmol]$ is Avogrado's number. The terms on the right-hand side of the equations correspond to the thermophoretic transport and the source terms. Thermophoresis is the physical phenomenon whereby soot particles in presence of a temperature gradient are driven towards lower temperature zones. The contribution of this phenomenon to the net transport velocity is accounted for through the inclusion of the thermophoretic velocity $V_{t,i}$, calculated as in Eq. (3).

$$V_{t,i} = -0.54 \frac{\mu}{\rho} \cdot \frac{1}{T} \cdot \frac{\partial T}{\partial x_i} \tag{3}$$

The expressions for the soot source terms are shown in Eqs. 4 and 5.

– Soot mass fraction source term $\dot{\omega}_s^{''}$:

$$\dot{\omega}_s^{''} = M_s \left[\underbrace{k_1(T)\,[C_2H_2]}_{\text{nucleation}} + \underbrace{k_2(T)\,f(S)\,[C_2H_2]}_{\text{surface growth}} - \underbrace{k_3(T)\,S\,[O_2]}_{\text{oxidation}} \right] \left[\frac{kg}{m^3 \cdot s} \right] \tag{4}$$

– Soot particle number density source term $\dot{\omega}_n^{''}$:

$$\dot{\omega}_n^{''} = \frac{1}{N_A} \left[\underbrace{\frac{2}{C_{min}} N_A k_1(T)\,[C_2H_2]}_{\text{nucleation}} - \underbrace{2C_a \left(\frac{6M_s}{\pi \rho_s} \right)^{1/6} \left(\frac{6\kappa T}{\rho_s} \right)^{1/2} C_s^{1/6}\,[\rho n]^{11/6}}_{\text{coagulation}} \right] \left[\frac{kmol}{m^3 \cdot s} \right] \tag{5}$$

where $C_{min} = 100$ is the number of carbon atoms in a nascent soot particle, $C_a = 9.0$ is an agglomeration rate constant, $\kappa = 1.38 \cdot 10^{-23}\,[J/K]$ is the Boltzmann constant, $\rho_s = 2000\,\left[kg/m^3\right]$ is the soot density, $M_s = 12.011\,[Kg/Kmol]$ is the soot molar mass, S is the soot surface area per unit volume and $C_s = \rho Y_s / M_s$ is the soot concentration. The reaction rates $k_i(T)$ are of the form $k_i(T) = A_i T^{n_i} e^{-T_i/T} [s^{-1}]$ and the constants A_i, n_i and T_i are shown in Table 1. The function $f(S)$ expresses the dependence of the surface growth term on soot surface area, here $f(S) = \sqrt{S}$.

The source terms describe the physico-chemistry of soot, where four stages are identified:

(i) **Nucleation:** inception of a new soot particle from its precursos (acetylene here).

(ii) **Surface growth:** increase in mass of soot particles due to the addition of carbon by chemical reactions occurring on the particles surface.

(iii) **Coagulation:** binding of two soot particle to form a bigger one.

(iv) **Oxidation:** consumption of soot mass by oxidizing species on the soot particle surface.

2.3. *Numerical tools and solution procedure*

To address soot modeling, three codes are sequentially used in this work:

First, the open source software *CANTERA* [20] is used to compute one-dimensional premixed and diffusion flames, allowing to obtain temperature, velocity and chemical species profiles. To model the gas-phase chemistry, the UDEL mechanism [21] is used, which considers 911 reactions and 70 species. It is able to predict sufficiently well the soot precursors level (acetylene in this case) at a reasonable computational cost.

Second, a numerical code, *CAN2SOOT*, solves the transport equations for the soot variables in one-dimensional premixed and counterflow diffusion flames on non-uniform meshes [22]. A first order finite differences spatial discretization is used. Temperature and species profiles of the flames are the ones given by *CANTERA*. The steady-state solution is obtained integrating the equivalent pseudo-transient problem with a first order (Euler's method) temporal scheme until convergence is reached.

Finally in the cases where radiation is considered, the discrete ordinates method (DOM) code *PRISSMA* [23,24,25] is used. *PRISSMA* tackles the problem of long distance thermal exchanges by solving the radiative transfer equation (RTE), where both emission and absorption of radiation are taken into account.

Radiation absorption within the medium is particularly important in the presence of soot, due to its strong radiative absorption. Only H_2O, CO_2, CO and soot are considered as radiative species and the detailed spectral model SNBcK [26] is used. An expression for the spectral absorption coefficient of soot is taken from Liu *et al.* [17]

CANTERA is used to compute the flame structure (only gas phase, no radiation). Then, soot profiles corresponding to each flame are calculated using *CAN2SOOT*. Soot is computed without taking into account the consumption of soot precursors within the flame.

When radiation is included in the computations, the three numerical tools *CANTERA*, *CAN2SOOT* and *PRISSMA* are used sequentially as shown in Fig. 1 to compute the flame structure, the soot volume fraction profiles and the radiative source term respectively. The 1D solution from *CAN2SOOT* is interpolated onto a 2D mesh which is then extruded to produce a rectangular 3D solution compatible with the radiative solver. *PRISSMA* calculates the radiative source term (S_r) which expresses the net volumetric energy gain due to the balance between the emitted and the absorbed radiation per unit of time. Appropriate boundary conditions are used for the calculation of radiation: perfectly absorbing boundary conditions at T=300 K are imposed at the fuel and oxidizer inlet planes whereas pseudo-periodic (reflecting) boundary conditions are set on the four planes corresponding to the burnt gas outflow, as sketched in Fig. 2.

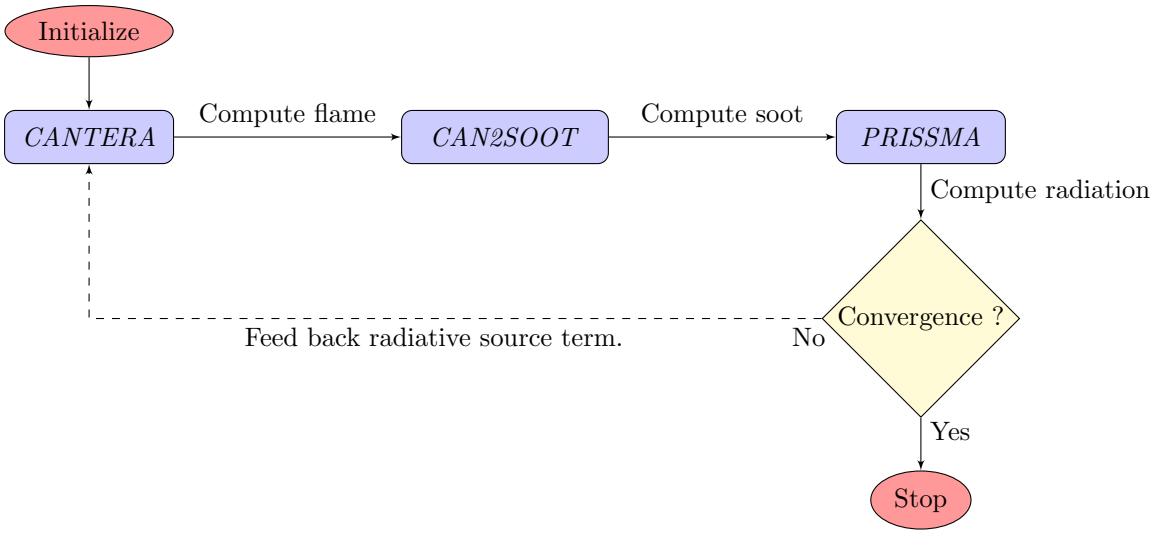

Figure 1. Flow chart of the solution procedure.

The calculated radiative source term along the central axis is then fed back to *CANTERA*, which plugs it in the energy equation to account for the volumetric power gain/loss. This sequence is repeated until convergence of the solution is attained, in this case when the relative change in soot volume fraction peak is lower than 10^{-5}, as proposed by Liu *et al.*[17]. This procedure leads to a fully gas phase/soot/radiation coupled solution.

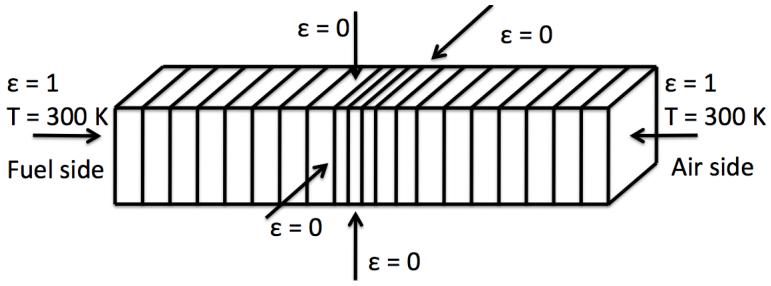

Figure 2. Sketch of the 3D solution of the flame including soot distribution given to *PRISSMA* and the boundary conditions used for the calculation of radiation, where ϵ refers to the emission coefficient at the boundaries.

3. Results

Simulations are performed in two ways: without radiation (Section 3.1) with radiation effects (Section 3.2).

3.1. *Non-radiative cases*

3.1.1. *Preliminar results*

Several ethylene/oxygen/nitrogen counterflow diffusion flames with varying oxygen content in the oxidizer stream have been computed in *CANTERA* using the UDEL mechanism. This set of flames was reported by Hwang & Chung [14], where profiles of soot volume fraction were measured. They are referred to as SF (soot formation) flames since the effect of soot oxidation is small for this particular set of flames. The number following the SF notation indicates the oxygen volume content in the oxidizer stream.

Figure 3 shows the calculated temperature T and the acetylene mole fraction X_{C2H2} corresponding to the SF flames. As the oxygen content in the oxidizer stream increases, the peak values of T and X_{C2H2} also increase.

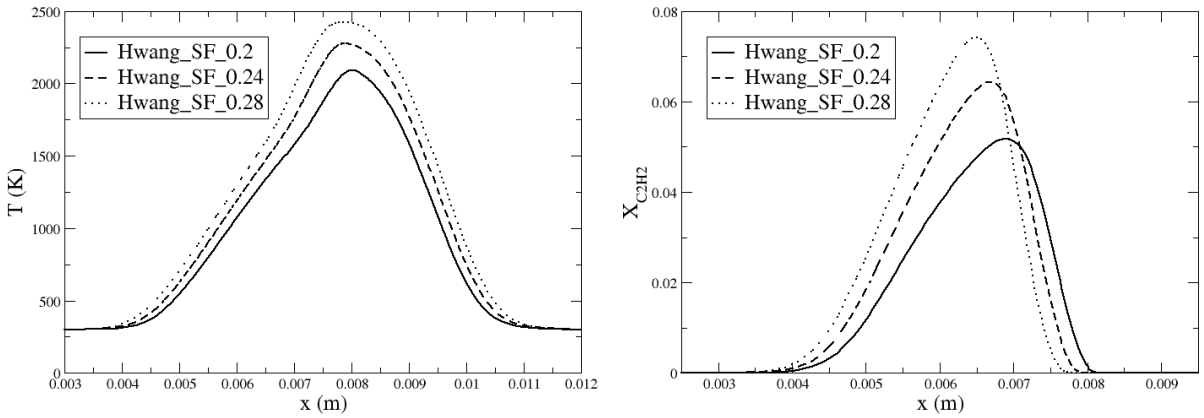

Figure 3. Calculated profiles corresponding to the Hwang & Chung flames. (a) Temperature. (b) Acetylene mole fraction.

Figure 4 compares the computed soot volume fraction profiles ($f_v = \rho Y_s/\rho_s$) in the three SF flames using the original Leung *et al.* model (hereafter referred to as LM1) in *CAN2SOOT* with the measurements of Hwang & Chung [14] and those of Vandsburger *et al.* [27]. Note that the experiments by Vandsburger *et al.* slightly differ from those of Hwang & Chung in the stretch rate, which does not alter the comparisons [17].

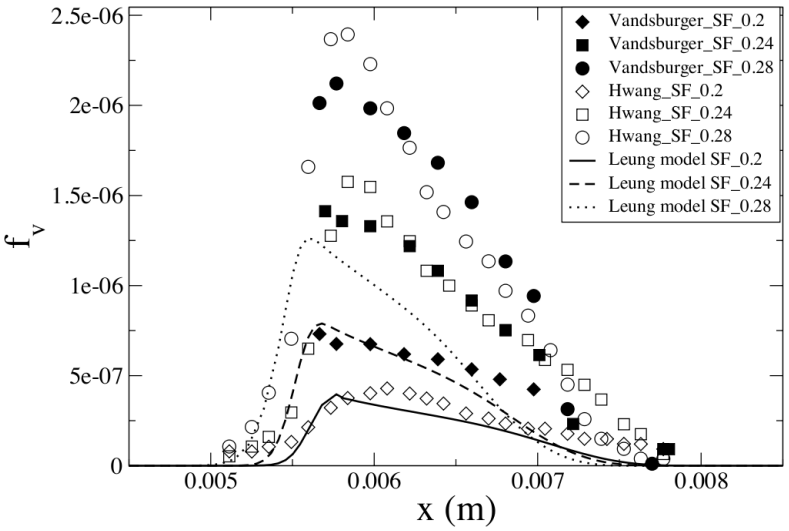

Figure 4. Soot volume fraction profiles on the SF flames configuration. Comparison between two sets of measurements [27,14] measured and computed soot volume fractions on the SF flames configuration using the LM1 model.

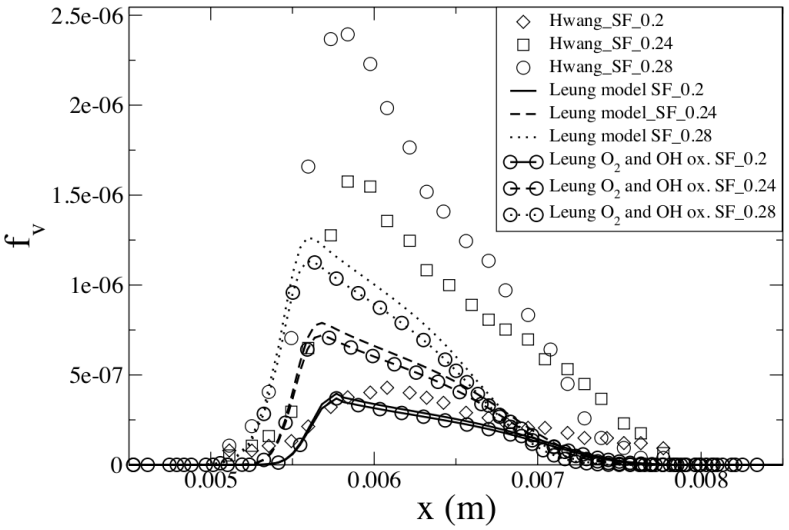

Figure 5. Soot volume fraction profiles on the SF flames configuration. Comparison between experiments of Hwang & Chung [14], numerical results using the original Leung *et al.* model and numerical results using the LM2 model.

The agreement between measurements and computation is reasonable. The profile shapes are correctly predicted, although the computed soot peak values are underpredicted by a factor of two with respect to the experiments in the SF_0.24 and SF_0.28 flames. This result is ascribed to the fact that the chemical

mechanism used throughout this work is not the same one used by Leung *et al.*. As the model constants depend on the chemical mechanism they must be adjusted to retrieve the experimental values.

Oxidation by OH is important [28] and its inclusion in the model is deemed necessary [10,29]. An additional oxidation term by OH as proposed by Liu *et al.* [16] is included in the original model (the original Leung *et al.* model with the additional OH oxidation term is referred to here as LM2 model). Soot profiles are again calculated in the SF flame configuration, the results are shown in Fig. 5. Predicted peak values of soot volume fraction decrease about 10% for the SF_0.28 flame with respect to the computation with oxidation only due to O_2. This difference would be more important if the predicted soot levels were higher. The effect of the OH oxidation is lower for flames with lower oxygen index, as less soot is produced.

3.1.2. *Adjustment of the soot model*

Calculations corresponding to the SF flames have been performed where, in order to retrieve the experimental soot levels, a modification in the surface growth term pre-exponential constant is proposed. The constant has been adjusted so as to retrieve the soot volume fraction peak value in the SF_0.28 flame including oxidation by both O_2 and OH and it takes a value of $A_2 = 1.04 \cdot 10^4$. This modified model is referred to as LM3 model. Results of the computations with the adjusted constant value are shown in Fig. 6. The fitted value of A_2 leads also to fairly good predictions of soot volume fraction in the SF_0.24 flame. Nonetheless, soot is overpredicted in the SF_0.2 flame. This disagreement has been reported previously [17], where it is suggested that the experimental values corresponding to the SF_0.2 flame should be taken with caution.

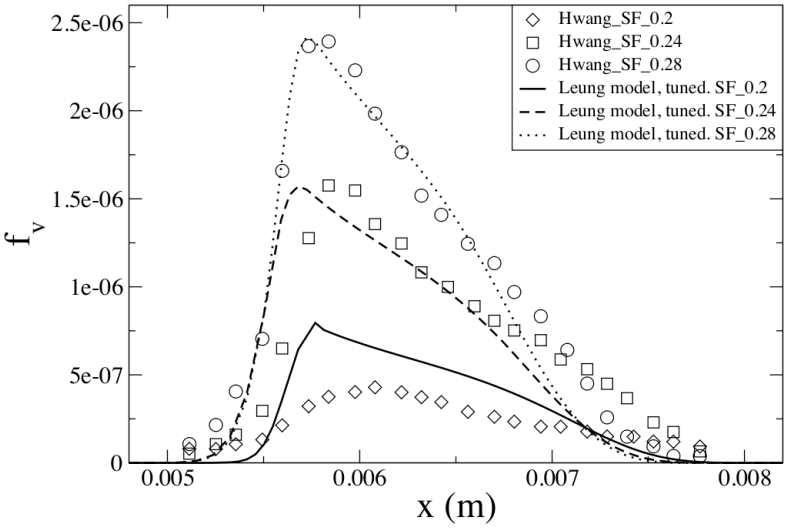

Figure 6. Soot volume fraction profiles in the SF flames configuration. Comparison between the experiments and the LM3 model.

3.2. *Soot/gas/radiation interaction*

In this section, the iterative procedure proposed in Section 2.3 is used with the LM3 model.

Figure 7 shows the profiles of temperature difference $\Delta T\left(x\right) = T\left(x\right)_{rad} - T\left(x\right)_{no\_rad}$ for the three SF flames, where $T\left(x\right)_{no\_rad}$ is the temperature computed without accounting for radiation and $T\left(x\right)_{rad}$ is the temperature computed with radiation. When gas and soot radiation contributions are included in the calculation, temperature drops of up to $20K$, $25K$ and $120K$ in the SF_0.2, SF_0.24 and SF_0.28 flames respectively are observed. The flame peak temperature drops by about 1% of their values. The impact of radiation in these flames is not very important due to tthe small volume of the domain. However, this effect may increase significantly in larger systems.

The computed profiles of radiative source term S_r for the SF_0.28 flame are represented in Fig. 8 for three different cases. The first one corresponds to a calculation where only radiation due to the gas phase is included. Note that the radiative source term is calculated in a postprocessing stage, there is therefore no feedback of radiation to the flame. The single bump corresponds to the net energy exchange (emission-absorption) between the hot gases and the cold surroundings. Positive values of S_r correspond to a power loss (net emission). A second calculation is shown, in which soot-driven radiation is included without closing the loop from Fig. 1. This allows to compute the corresponding S_r profile, where no radiation feedback on the flame is accounted for. In addition to the radiation due to the hot burnt gases, a second bump appears, due to the presence of soot. The third profile shows the radiative source term corresponding to the coupled solution procedure. The soot-driven radiation bump is decreased. The effect that radiation has on soot is to decrease the amount of soot produced, due to the temperature drop induced by the radiative heat loss.

Figure 9 shows the computed soot volume fraction profiles in the SF flames, with and without radiation. As mentioned above, it is observed that when gas and soot radiative losses are introduced, a decrease in the soot volume fraction peak of $\sim 6\%$ is observed for the three flames studied. Soot formation seems to be slightly affected by radiative losses. The methodology proposed provides, however, a framework in which more complicated soot formation and chemistry models can be tested. In particular, models based on PAH soot formation and growth might be a good alternative as the impact of temperature on soot precursors, and therefore on soot formation, might be more important.

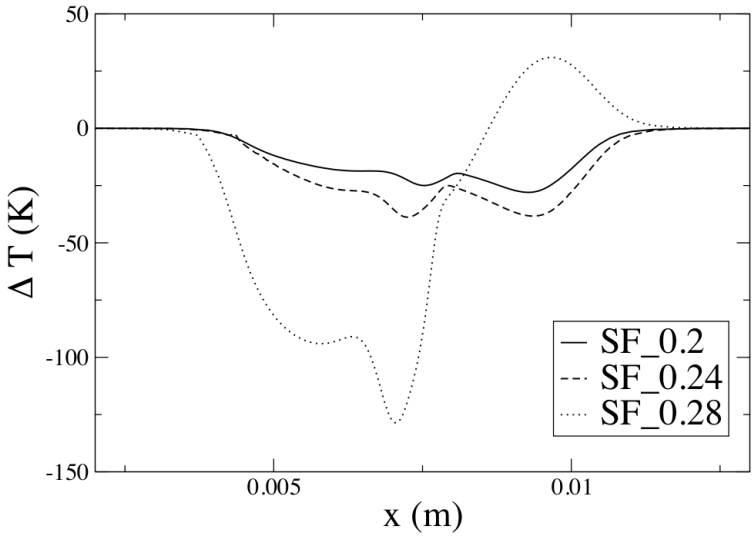

Figure 7. Profiles of temperature difference $\Delta T\left(x\right) = T\left(x\right)_{rad} - T\left(x\right)_{no\_rad}$ in the SF flames configuration using LM3 model.

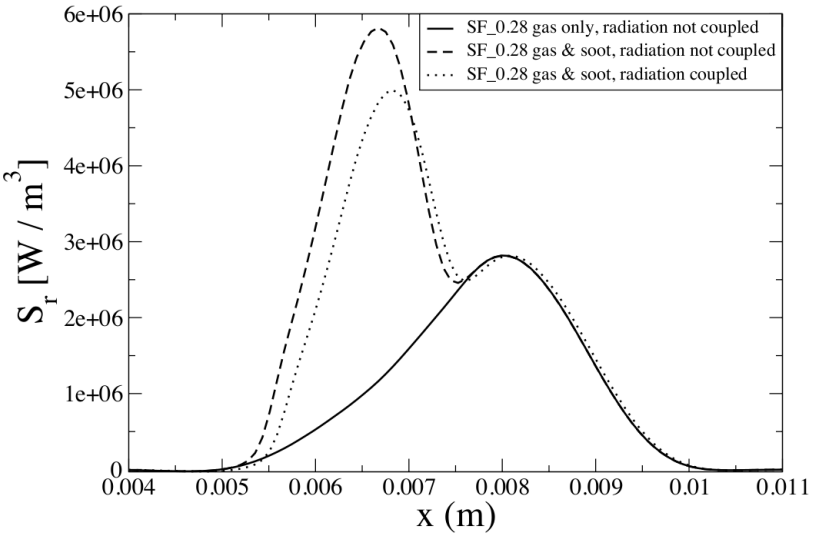

Figure 8. Computed radiative source term in the SF flames configuration. Three curves are shown: soot was not computed, no feedback from radiation to the flame (solid line); soot was included using LM3 model, no feedback from radiation to the flame (dashed line); soot was included using LM2 model, feedback from radiation to the flame (dotted line).

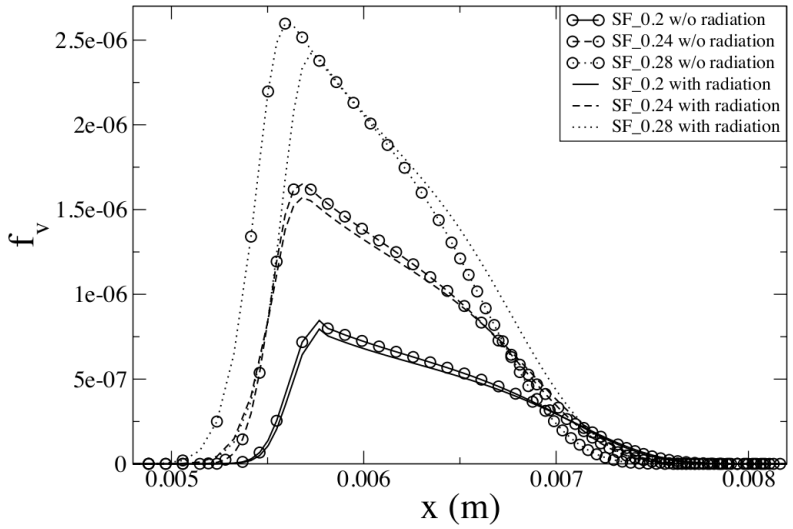

Figure 9. Profiles of soot volume fraction in the SF flames configuration with and without radiation using LM2 model.

4. Conclusion

A methodology has been proposed to compute soot in one-dimensional flames where radiation is taken into account. A set of ethylene/air counterflow diffusion flames has been calculated using a detailed chemical mechanism. Later on, soot produced in these flames has been computed using a two-equations semi-empirical model with a one-dimensional code developed for this purpose. Higher soot levels were

found in the flames with higher levels of soot precursors (acetylene) and higher peak temperature, the results being qualitatively in accordance with experimental results. The soot model was then adjusted to retrieve the soot levels measured experimentally in one of the flames, and yielded quantitatively good predictions for the rest of the flames. Finally, a radiation code was used to perform fully coupled simulations of the gas phase, soot and radiation in the flames studied. Radiation emitted by soot was found to be very important with respect to that due to the gas phase. It was observed that the effect of soot-driven radiative losses is to lower the peak temperature of the flames and to lower the soot level itself because of the decrease in temperature. However, radiative losses induce small temperature drops in the flames studied. The results obtained are in accordance with those from previous studies [17,18].

The methodology presents all the necessary blocks to allow for a systematic testing of different soot models and the interaction with radiation. It is a tool susceptible of improvements due to its modularity and flexibility. The inclusion of more sophisticated soot models taking into account the formation and growth of soot by PAH's is proposed for future studies. Also, the soot models tested might be implemented into 3D solvers for the prediction of soot in complex geometries using reduced chemical mechanisms and a tabulated chemistry for the soot precursors and oxidizing species.

Acknowledgements

The authors gratefully acknowledge the financial support by the European Commission, within the Marie Curie Actions - Initial Training Networks, under call FP7-PEOPLE-2007-1-1-ITN, LIMOUSINE project with number 214905.

References

[1] K. M. Leung and R. P. Lindstedt. A simplified reaction mechanism for soot formation in nonpremixed flames. *Combust. Flame* , 87:289–305, 1991.

[2] G. Blanquart, P. Pepiot-Desjardins, and H. Pitsch. Chemical mechanism for high temperature combustion of engine relevant fuels with emphasis on soot precursors. *Combust. Flame* , 156:588–607, 2008.

[3] M.E. Mueller, G. Blanquart, and H. Pitsch. Hybrid method of moments for modeling soot formation and growth. *Combust. Flame* , 156(6):1143–1155, June 2009.

[4] B. Kärcher, O. Möhler, P. J. DeMott, S. Pechtl, and F. Yu. Insights into the role of soot aerosols in cirrus clouds formation. *Atmospheric Chemistry and Physics*, 7:4203–4227, 2007.

[5] H. Jung, B. Guo, C. Anastasio, and I. M. Kennedy. Quantitative measurements of the generation of hydroxyl radicals by soot particles in a surrogate lung fluid. *Atmospheric Environment*, 40(6):1043–1052, 2006.

[6] R. Viskanta and M. P. Mengük. Radiation heat transfer in combustion systems. *Prog. Energy Comb. Sci.* , 13:97–160, 1987.

[7] Ian M. Kennedy. Models of soot formation and oxidation. *Prog. Energy Comb. Sci.* , 23:95–132, 1997.

[8] N J. Brown, K. L. Revzan, and M. Frenklach. Detailed kinetic modeling of soot formation in ethylene/air mixtures reacting in a perfectly stirred reactor. *Twentieth Symposium (International) on Combustion*, 27:1573–1580, 1998.

[9] B. S. Haynes and G. Gg. Wagner. Soot formation. *Prog. Energy Comb. Sci.* , 7:229–237, 1981.

[10] J.B. Moss, C.D. Stewart, and K.J. Young. Modeling soot formation and burnout in a high temperature laminar diffusion flame burning under oxygen-enriched conditions. *Combust. Flame* , 101:491–500, 1995.

[11] C. W. Lautenberger, J. L. de Ris, N. A. Dembsey, J. R. Barnett, and H. R. Baum. A simplified model for soot formation and oxidation in CFD simulation of non-premixed hydrocarbon flames. *Fire Safety Journal*, 40:141–176, 2005.

[12] T. Beji, J. P. Zhang, W. Yao, and M. Delichatsios. Validation of a novel soot model in laminar diffusion flames: fuel, flow rate and thermophoretic effects. In The Combustion Institute, editor, *Sixth Mediterranean Combustion Symposium*, 2009.

[13] T. Beji, J.P. Zhang, W. Yao, and M. Delichatsios. A novel soot model for fires: validation in a laminar non-premixed flame. *Combust. Flame* , 158(2):281–290, 2010.

[14] J. Y. Hwang and S. H. Chung. Growth of soot particles in counterflow diffusion flames of ethylene. *Combust. Flame* , 125:752–762, 2001.

[15] M. D. Smooke, I. K. Puri, and K. Seshadri. A comparison between numerical calculations and experimental measurements of the structure of a counterflow diffusion flame burning diluted methane in diluted air. *Proc. Combust. Inst.* , 21:1783–92, 1986.

[16] F. Liu, H. Guo, G. J. Smallwood, and Ö. L. Gülder. Effects of gas and soot radiation on soot formation in a coflow laminar ethylene diffusion flames. *J. Quant. Spect. and Radiative Transfer* , 73:409–421, 2002.

[17] F. Liu, H. Guo, G. J. Smallwood, and M. El Hafi. Effects of gas and soot radiation on soot formation in counterflow ethylene diffusion flames. *J. Quant. Spect. and Radiative Transfer* , 84:501–511, 2004.

[18] H. Guo, F. Liu, and G. J. Smallwood. Soot and NO formation in counterflow ethylene/air/nitrogen diffusion flames. *Combust. Theory and Modelling* , 8:475–489, 2004.

[19] H. T. Brocklehurst, J. B. Moss, C. D. Hurley, and C. H. Priddin. Soot and radiation modeling in gas turbine combustion chambers. In *RTO AVT Symposium on "Gas Turbine Engine Combustion, Emissions and Alternative Fuels"*, 1998.

[20] D.G.Goodwin. *Cantera C++ Users Guide*. http://sourceforge.net/pro jects/cantera, 2002.

[21] S. G. Davis, C. K. Law, and H. Wang. Propene pyrolysis and oxidation kinetics in a flow reactor and laminar flames. *Combust. Flame* , 119:375–399, 1999.

[22] I. Hernández. *Soot modeling and Large-Eddy Simulations of thermo-acoustic instabilities*. PhD thesis, INP Toulouse, 2011.

[23] J. Amaya, O. Cabrit, D. Poitou, B. Cuenot, and M. El Hafi. Unsteady coupling of Navier-Stokes and radiative heat transfer solvers applied to an anisothermal multicomponent turbulent channel flow. *J. Quant. Spect. and Radiative Transfer* , 111(2):295–301, January 2010.

[24] D. Poitou, M. El Hafi, and B. Cuenot. Analysis of radiation modeling for turbulent combustion: development of a methodology to couple turbulent combustion and radiative heat transfer in les. *J. Heat Trans.* , 133, 2011.

[25] D. Poitou, J. Amaya, M. El Hafi, and B. Cuenot. Analysis of the interaction between turbulent combustion and thermal radiation using unsteady coupled les/dom simulations. *Combust. Flame* , 2011.

[26] V. Goutière, A. Charette, and L. Kiss. Comparative performance of non-gray gas modeling techniques. *Numerical Heat Transfer Part B: Fundamentals*, 41:361–381, 2002.

[27] U. Vandsburger, I. M. Kennedy, and I. Glassman. Sooting counterflow diffusion flames with varying oxygen index. *Combust. Sci. Tech.* , 39:263–285, 1984.

[28] C.P.Fenimore and G.W.Jones. Oxidation of soot by hydroxyl radicals. *J. Phys. Chem*, 71:593–597, 1967.

[29] O. A. Ezekoye and Z. Zhang. Soot oxidation and agglomeration modeling in a microgravity diffusion flame. *Combust. Flame* , 110:127–139, 1997.

Table 1
Leung's soot model constants.

A_1	A_2	A_3	n_1	n_2	n_3	$T_1\,[K]$	$T_2\,[K]$	$T_3\,[K]$
$0.1 \cdot 10^5$	$0.6 \cdot 10^4$	$0.1 \cdot 10^5$	0	0	0.5	21100	12100	19680